Magnetization reversal via single and double vortex states in submicron Permalloy ellipses

P. Vavassori,[1] N. Zaluzec,[2] V. Metlushko,[3] V. Novosad,[2] B. Ilic,[4] and M. Grimsditch[2]
[1]*INFM-National Research Center for Nanostructures and Biosystems at Surfaces* (S^3), *Dipartimento di Fisica, Universita de Ferrara, Ferrara, Italy*
[2]*Materials Science Division, Argonne National Laboratory, Argonne, Illinois 60439, USA*
[3]*Department of Electrical and Computer Engineering, University of Illinois at Chicago, Chicago, Illinois 060607, USA*
[4]*Cornell Nanofabrication Facility and School of Applied Engineering and Physics, Cornell University, Ithaca, New York, USA*
(Received December 5, 2003; published 3 June 2004)

The magnetization reversal mechanism in an array of submicron elliptical Permalloy elements with an aspect ratio 1.4:1 is investigated using the diffracted magneto-optic Kerr effect technique, Lorentz scanning transmission electron microscopy, and Lorentz transmission electron microscopy. The experimental results are interpreted from a comparison with micromagnetic simulations. The reversal mechanism is found to be dependent on the direction of the magnetic field and to occur via the formation of one or two vortices; the one vortex state is nucleated when the field is applied along the short axis. For the field applied along the long axis a mixture of one- and two-vortex states is observed at remanence.

DOI: 10.1103/PhysRevB.69.214404 PACS number(s): 75.75.+a, 75.60.Jk, 78.20.Ls

INTRODUCTION

Magnetization reversal in submicron size dot particles is one of the key issues crucial for applications in data storage. One difficult task in such small magnetic structures is to control their magnetization reversal, which is very dependent on the constituent material, size and shape, edge roughness, etc. In addition to the technological interest, there is also interest from a fundamental standpoint geared towards understanding and modeling the magnetic behavior of individual sub-micrometer ferromagnetic particles and of arrays of interacting particles. If the length scale of these particles is sufficiently small, then their magnetic properties can deviate substantially from the magnetic response of the bulk material. In particular, it is possible for the shape of the particle to be the dominant factor in determining the magnetic response of these elements. Numerous investigations have addressed this issue and the related issue of the domain structure at remanence.[1] However, due to the continuous improvement of the size and shape control offered by modern lithographic techniques, novel magnetic behavior is continuously being reported and making it clear that magnetism at the nanoscale is not yet fully understood.

In the case of magnetically soft materials, in which the crystalline anisotropy can be neglected, the magnetization reversal process and field evolution of the spin structure greatly depends on the shape and geometrical aspect ratio of the particle. Micromagnetic simulations of elliptically shaped Permalloy particles reveal that one-, two- or three-vortex states can be stabilized in remanence.[2] All three states are found to have comparable energies. The border of stability of each state depends on the particle aspect ratio. In general, multivortex states can reduce the number of vortices by expelling a vortex from the particle under the effect of a suitable external magnetic field. For example, the transition from a two-vortex to a single vortex state, induced by the magnetic field of the probe used for magnetic force microscopy (MFM) imaging, was recently reported.[3]

In this investigation we have used the diffracted magneto-optic Kerr effect (DMOKE) technique and Lorentz electron microscopy to study the magnetization reversal in an array of elliptical Permalloy elements with an in-plane aspect ratio of 1.4:1. The DMOKE technique exploits the diffracted beams produced by the array when the wavelength of the incident light is comparable to the period of the array.[4–8] These investigations demonstrated that DMOKE is a powerful tool to address the mechanism of magnetization switching and to study domain formation during the reversal process. Analysis of the diffracted loops shows the formation and annihilation of a single vortex state structure when the field H is applied along the short axis of the ellipses. Instead, when the field H is applied along the long axis of the ellipses, the reversal process includes the nucleation and annihilation of a two-vortex structure. Images obtained at remanence using Lorentz scanning transmission and Lorentz transmission electron microscopy,[9,10] show the coexistence of the one and two vortex states. The MOKE technique has also been used to study the angular dependence of the one- and two-vortex nucleation and annihilation processes.

EXPERIMENTAL

The sample fabrication process begins with the deposition/growth of low stress silicon nitride on both sides of a standard double polished (100) silicon wafer. A layer of optical photoresist is applied to the bottom side of the wafer and the window pattern was exposed. The window was etched entirely through the silicon, leaving a suspended nitride ''window membrane'' of 400 μm$\times$400 μm and 50 nm thick on the front of the wafer. The double-layer *e*-beam resist was applied to the front side of the wafer and a thin layer of gold was evaporated on the top to prevent accumulation of charge from the electron beam. The pattern of ellipses was written with *e*-beam lithography, developed, and a 50 nm permalloy film was deposited by *e*-beam deposition in high vacuum. After lift-off in acetone the array of 50 nm thick elliptical dots of permalloy, arranged on a square lattice with a period of 1 μm, was obtained. The resulting ellipses

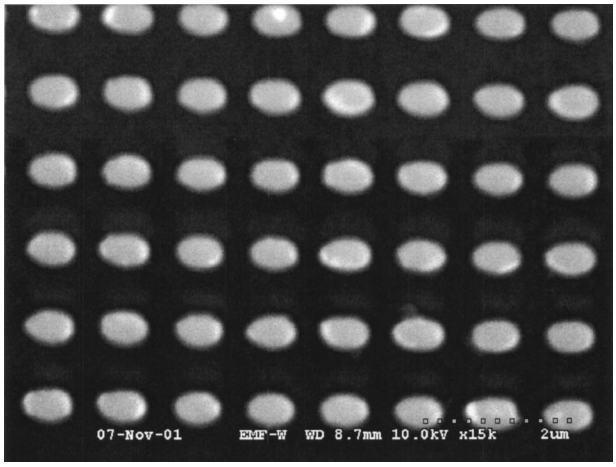

FIG. 1. Scanning electron microscopy image of the sample.

were found to be slightly smaller on the free standing silicon nitride window than in the area with the Si substrate: this can be traced to backscattered secondary electrons from the Si substrate during the writing step. A scanning electron microscopy image of the sample on the window is shown in Fig. 1; the major and minor axes are 685 and 485 nm, respectively. In the rest of the array the ellipse axes are 820 and 580 nm. Due to curvature of the silicon nitride window and multiple reflection effects from the top and bottom surfaces MOKE measurements performed on the silicon nitride window area were too noisy for suitable analysis. The MOKE results presented here were performed on the array with the Si substrate. Since the Lorentz images are taken on the silicon nitride window portion, the size differences do play a role in the data analysis.

The DMOKE measurements were carried out with the incident beam polarized in the plane of incidence (p polarization) and the magnetic field is applied perpendicularly to the plane of incidence, as described in Ref. 4. This arrangement corresponds to the transverse MOKE geometry where the changes in the sample magnetization lead to changes in the intensity (I) of reflected and diffracted beams, leaving their polarization state unchanged.

Lorentz microscopy images were carried out in the ANL FEG AAEM (Ref. 11) as well as a FEI Tecnai F20 TEM/STEM instruments. In these instruments, the electron optical column was operated in a zero field mode, where the objective lens is turned off and the probe forming lens functions were reallocated to the pre-specimen Condensor (C1, C2, and C3) lenses. Post specimen lenses (P1, P2, P3, P4) were used to magnify the Lorentz scattered electrons to either CCD detectors or conventional bright field and annular dark field detectors. Lorentz scanning transmission (LSTEM) images were formed by allowing the Lorentz signal to modulate and produce the image through the various post specimen detectors. Lorentz transmission electron microscopy (LTEM) images where formed using the Fuller and Hale[10] methods.

RESULTS AND DISCUSSION

Figure 2 shows the measured (left panels) and calculated (right panels) hysteresis loops in the 0th through second diffraction orders with the external field H applied along the long axis. Figure 3 contains the hysteresis loops for the field along the short axis. On their own, neither the measured loops nor the micromagnetic simulations enable the reversal mechanism to be extracted reliably. The experimental loops require modelling in order to be interpreted; the simulations can seldom guarantee that all subtle shape and history effects have been accounted for. However, the qualitative differences between the loops for the two field directions indicate that reversal is occurring via a different mechanism. The micromagnetic simulations show that the remanent state when the field is applied along the long axis is a two-vortex state while when field is along the short axis one vortex is observed at remanence. For decreasing fields the magnetization jump at the nucleation field ($H_n \approx 250$ and 600 Oe, for H along and perpendicular to the long axis, respectively) corresponds to the transition from the saturated single-domain state to a vortexlike magnetic state. The linear part of the loop, around $H \approx 0$, corresponds to reversible displacements of the vortexlike structure, and when the magnetic field

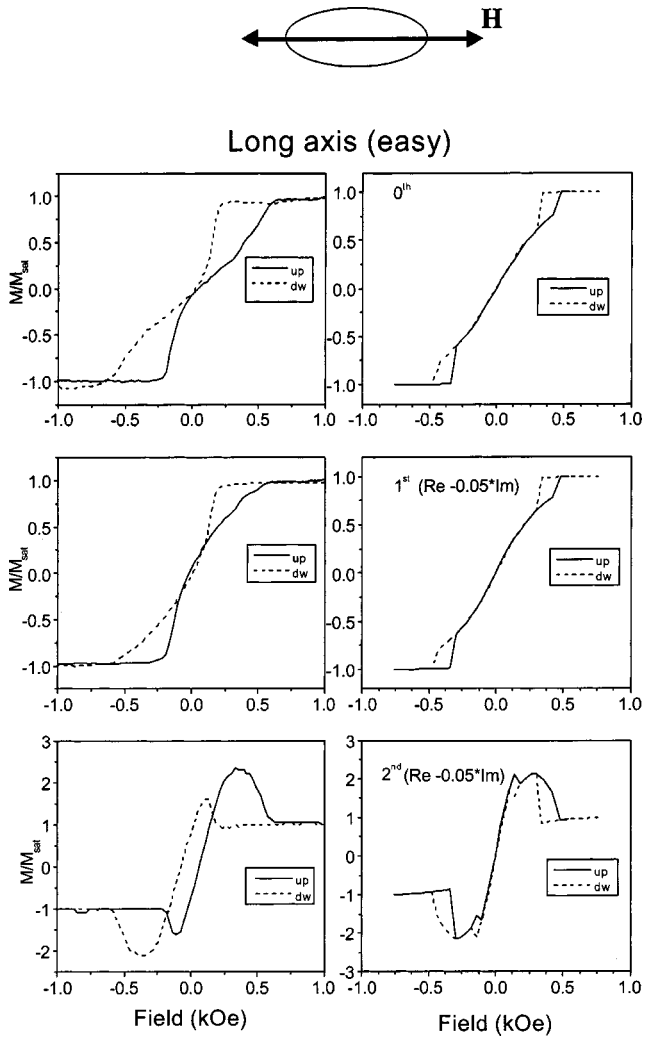

FIG. 2. Measured (left panels) and calculated (right panels) diffracted hysteresis loops of various orders with the external field applied parallel to the long axis of the ellipse.

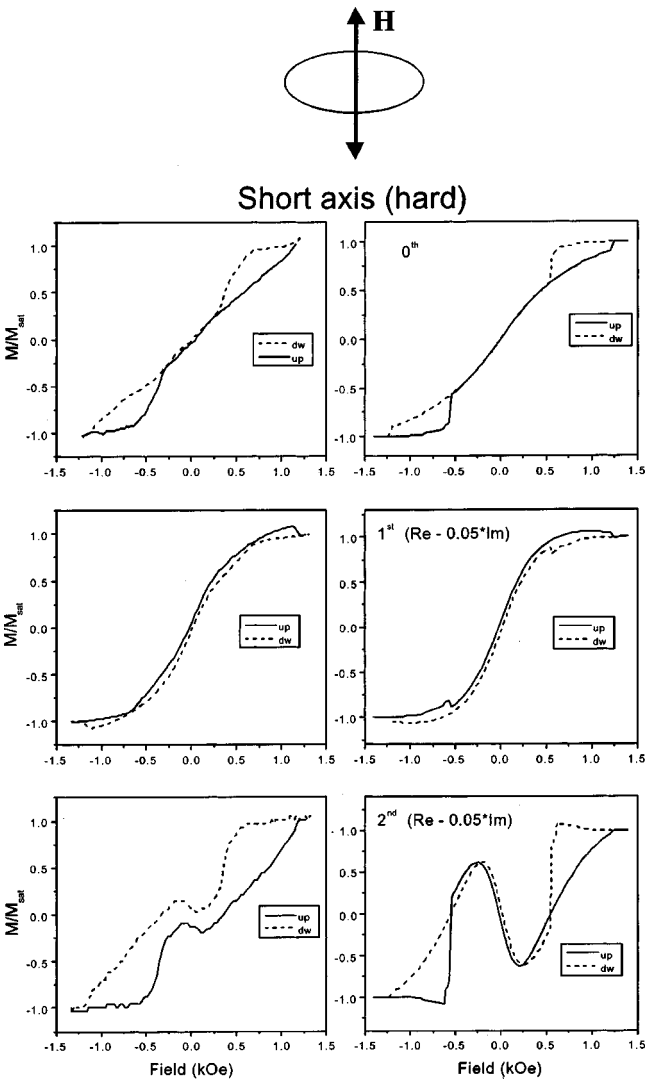

FIG. 3. Measured (left panels) and calculated (right panels) diffracted hysteresis loops of various orders with the external field applied parallel to the short axis of the ellipse.

reaches the annihilation field $H_{an} \approx 650$ and 1300 Oe, for the two directions of H, the vortexlike structure is swept out of the dot. The agreement between the calculated and measured loops, especially the first and second orders, confirms that the simulations indeed capture the essence of the reversal mechanisms.

In order to quantitatively interpret the loops in Figs. 2 and 3 we follow the approach given in Refs. 6–8. The magneto-optical contribution to the nth order diffracted beam is proportional to

$$\Delta I_m^n \alpha \{\mathrm{Re}[f_n^m] + A_n \,\mathrm{Im}[f_n^m]\}, \tag{1}$$

where f_n is the magnetic form factor and A_n is a parameter (in principle calculable), dependent on the diffraction order n and the optical and magneto-optical constants of Permalloy and the substrate.[8] Here we treat A as an adjustable parameter. The magnetic form factor is defined by

$$f_n^m = \int m_y \exp[in\mathbf{Gr}]dS, \tag{2}$$

where $\mathbf{G}$ is the reciprocal lattice vector of the array, m_y is the component of the magnetization perpendicular to the plane of incidence, and the integral is carried out over a unit cell of the array; in this case a single elliptical dot.

To obtain the field dependent magnetic form factors we have used the object oriented micromagnetic framework (OOMMF).[12] At each field the magnetization distribution is extracted and the form factors calculated via Eq. (2). The loops are then generated using Eq. (1). (The material parameters used for the calculation are those contained in the OOMMF program for Permalloy; $M_s = 8.6 \times 10^5$ A/m, $A = 1.3 \times 10^{13}$ J/m, $K = 0$.) The side of the cubic unit cell used in the computations was 5 nm.[13] In a few instances we performed calculations with 8, 5, and 3.5 nm cells; to confirm that no significant differences, due to the choice of the simulation cell size, were observed.

Many of the micromagnetic simulations were found to be very sensitive to subtle features of the simulation. The nucleation process was sometimes found to depend on the initial magnetization state. For example, a perfect collinear (uniform) magnetization state at high fields does not always lead to the same vortex state as starting from a vortex state, increasing the field to annihilate the vortex, and then decreasing the field to produce nucleation. In the latter case the particle retains a memory of its vortex state and tends to renucleate into the same structure. Even quite large fields above annihilation do not erase this memory. This is because the spin structure retains a slight asymmetry that may result in different nucleation modes. The inclusion of a small out of plane component of the field can also have profound effects on both nucleation and annihilation. Changes in cell size also affect the results of the simulations. The reason for the subtle variations in reversal path is the comparable energy of the metastable states[2] and the various nucleation paths that can be followed.[14] We will return to these issues when presenting our simulation results.

Figures 4 and 5 show the stable magnetic configurations at various points on the hysteresis curve obtained for the two directions of H. When the field H is applied along the long axis of the ellipses (easy direction), the simulations in Fig. 4 indicate reversal via the nucleation and annihilation of a two-vortex structure. Instead, when H is applied along the short axis of the ellipses (hard direction), the simulations in Fig. 5 show a magnetization reversal via the formation and annihilation of a single vortex. These conclusions are found to be independent of any subtle details of the micromagnetic simulations.

The form factors extracted from magnetic configurations such as those in Figs. 4 and 5 lead, via Eq. (1) with $A_n = -0.05$,[8] to the loops shown in the right-hand panels of Figs. 2 and 3. For all orders the salient features displayed by the measured loops are well reproduced by the calculated ones. Given the complexity of magnetization reversal, which can depend on edge roughness and deviations from ideal

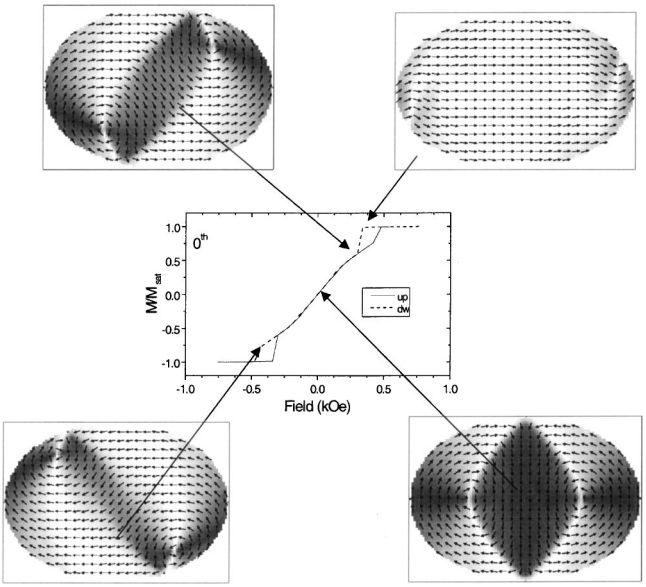

FIG. 4. Micromagnetic configurations calculated at different external fields applied along the long axis of the ellipse.

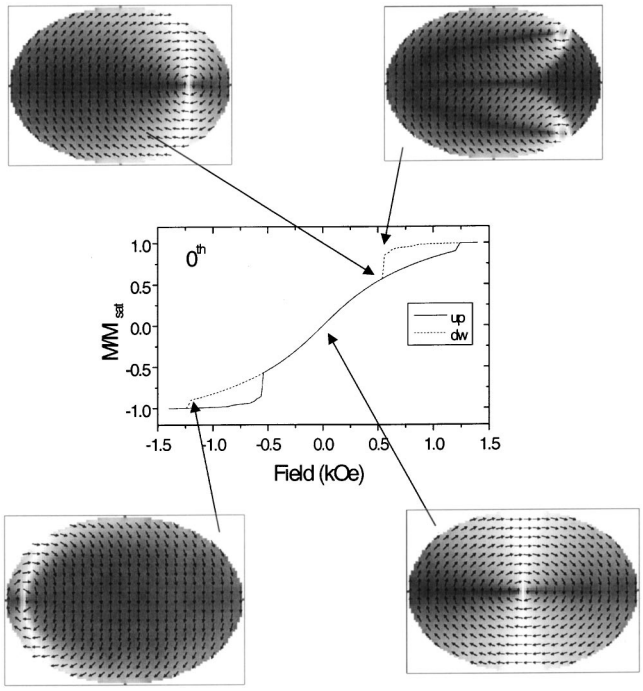

FIG. 5. Micromagnetic configurations calculated at different external fields applied along the short axis of the ellipse.

shape, it is reasonable to ascribe the differences between the experimental and calculated loops to a distribution of nucleation and annihilation fields.

The agreement between the features of the calculated and experimental loops for the two directions of field, especially for the second order loops, provides strong evidence for the existence of one- and two-vortex reversal mechanisms. It is interesting to consider in more detail the different micromagnetic evolution for H along the two directions. When H is applied along the long axis of the ellipse, the micromagnetic state that evolves into a double vortex, is an "*S*" state (upper right panel Fig. 4). This state retains a center of inversion symmetry but has already broken the left-right and top-bottom symmetries of the saturated state; why it chooses this path is an unresolved issue. The subsequent reversal mechanism maintains the center of inversion symmetry throughout. For H along the short axis, the seed state for reversal looks similar to a double "*C*" state (upper right panel Fig. 5); this configuration retains the top-bottom symmetry but has lost the left-right and inversion symmetries. The origin of this behavior is also not yet known. In the calculations symmetry breaking effects will be determined by numerical rounding errors, experimentally it is more likely to be governed by small imperfections in the particle shapes. From the double *C* state, two vortices are nucleated at the particle edge when H is reduced. However, for the field applied exactly along the short axis these two vortices are not stable and they merge into a single vortex with the core lying on the long axis of the ellipses and displaced with respect to the dot center (upper left panel Fig. 5). Surprisingly therefore the micromagnetic simulations indicate that two vortices nucleate for both directions of the field; in one case the two vortices have opposite chirality and do not merge, for the other field direction they have the same chirality and merge into a single vortex. These findings are consistent with the buckling spin instability, that results in the nucleation of magnetic vortices in elliptical particles, that has been previously studied analytically and with micromagnetic calculations.[14]

To investigate the evolution of reversal via one or two vortex states we recorded MOKE loops as a function of angle between the field and the long axis of the sample. The nucleation (circles) and annihilation (squares) fields extracted from those loops are shown in the upper panel of Fig. 6; the corresponding micromagnetic simulation results are shown in the lower panel. Because of the dramatic effects that subtle simulation details have on the reversal process the micromagnetic results require detailed explanation. We found that the nucleation fields are almost identical for the remanent single or double vortex states. So, even though the final state could be a one- or a two-vortex state, the values of nucleation field did not change appreciably. We did conclude, however, that for applied fields within roughly 30° of the long and short axes (viz. from 0° to 30° and from 60° to 90° in the lower panel of Fig. 6) the remanent states were single and double vortex states, respectively. Between 30° and 60° single or double vortex states could be obtained depending on the details of the calculation. Nucleation fields are shown by circles; filled circles indicate a two vortex state, open circles single vortices. Circles with a cross inside indicate that one or two vortex states are possible. Annihilation studies are in some sense easier since the single or double vortex states can be chosen as the starting configuration. For a single vortex the angular dependence of annihilation field is controlled by the uniaxial shape anisotropy and does not depend on any small parameter of the micromagnetic model. The results are shown by the solid squares in the lower panel of Fig. 6. Annihilation of a double vortex is more complex since it depends on the direction of the field relative to the orientation of the central part of the sample

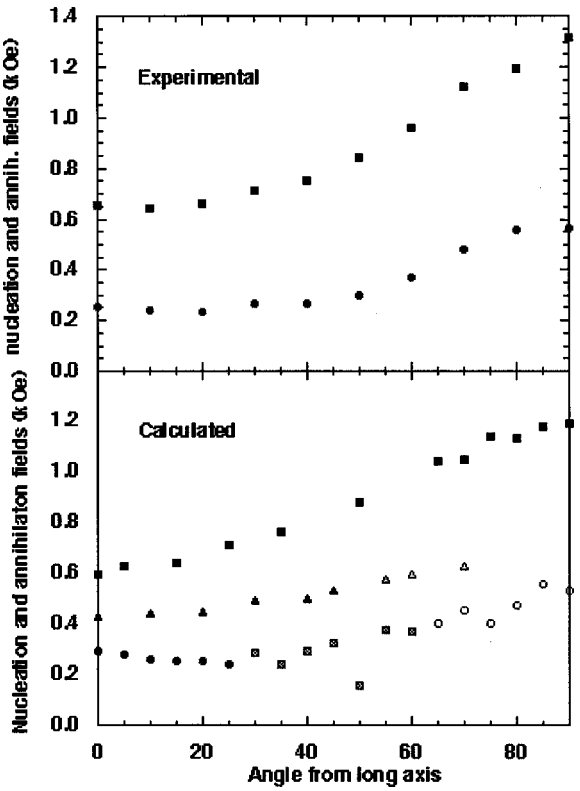

FIG. 6. The nucleation (circles) and annihilation (squares and triangles) fields measured (upper plot) and calculated (lower plot) for Permalloy elliptical $820\times580\times50$ nm^3 particles. The angle of zero degrees corresponds to the magnetic field aligned along the easy (long) axis.

(see bottom right of Fig. 4). In order to compare with experiment it can be shown that the relevant field direction must oppose the direction of the magnetization in the center (i.e., upwards in the bottom right of in Fig. 4). For angles below 45° the resulting annihilation fields are robust in the sense that they do not depend on small details—these are indicated by solid triangles. They correspond to simultaneous expulsion of both vortices. For larger angles two distinct annihilation process are observed (i) one vortex is expelled at a low field and the second one at the field expected for a single vortex (squares), (ii) both vortices are simultaneously expelled. The latter are indicated by open triangles in Fig. 6.

The calculated and measured nucleation fields in Figs. 6 are in good agreement both in their magnitude and their angular dependence: both span the range from 250 to 550 Oe. To compare the annihilation fields one must note that at small angles experimentally we expect to be in the two-vortex state (triangles in Fig. 6) but in the single vortex state (squares) when we approach 90°. The micromagnetics thus predicts changes from 450 to 1200 Oe while experimentally we measured 650 to 1300 Oe. It must be noted that while the nucleation field can be determined quite precisely from the measured loops, the annihilation field is not so well defined. This can explain the slight disagreement between the experimental and calculated annihilation field ranges. The experimental annihilation fields change smoothly with angle, without a sharp transition between one and two vortex processes.

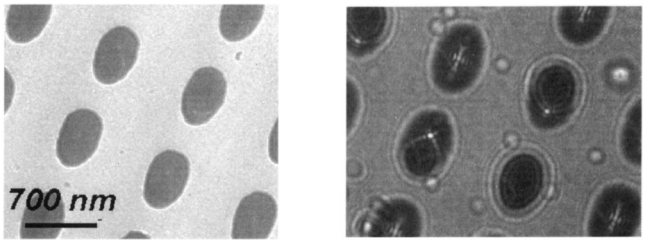

FIG. 7. Lorentz electron microscopy images of the remanence states in elliptical dots. (a) Conventional TEM image showing the ellipses in a saturated state. (b) Corresponding LTEM image of the remnant state, the magnification of the Lorentz image differs slightly from the infocus image due to the Lorentz mode.

This is not surprising considering the comparable energy of the metastable one- and two-vortex states in the intermediate angle range (30°–60°), so that even small asymmetries or imperfections in the particles are sufficient to randomly bias the reversal towards either the one- or two-vortex process. In this angular region, the most likely state for the whole system is expected to be a mixture of single and double vortices.

Using LSTEM and LTEM we have observed single and double vortex states. Figure 7(a) is the conventional image, while Fig. 7(b) is the Lorentz image showing a portion of the array containing both single and double vortex remanent states after having applied a high field parallel to the long axis of the ellipses. In order to facilitate the interpretation of Lorentz images we show, in Fig. 8, the image of two circular disks where a single vortex is known to be the stable remanent state. Taken in zero field, the bright and dark contrast (spots) in the center of each dot are produced by the circulating magnetization profile which ''focuses'' or ''defocuses'' the electrons depending on the vortex chirality. In the disks with a bright center spot one can also observe a dark ring on the outer edge; a bright ring is expected in the disks with dark centres but this is not visible. This correlation between the outer rings and the central spot greatly simplifies the interpretation of the elliptical dot mages. It can easily be seen that of the four complete ellipses in Fig. 7(b) the one with a white cross in the center and the one that is completely black are single vortex states with opposite chirality. (Again, the surrounding ring structure supports this interpretation.) Ellipses with a bright spot either above or below the center are in a two-vortex state—the dark spot at the symmetric position is inferred but note that the surrounding ''ring'' structure is consistent with this interpretation.

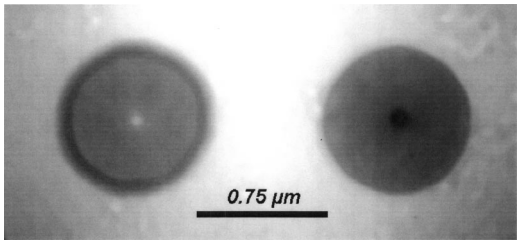

FIG. 8. Lorentz images of circular vortices with opposite chirality. The contrast reversal at the dot center (white to black) indicates the reversal of chirality. Note: the image contrast of this image has been stretched to facilitate observation of the weak Lorentz contrast, and minimize the background.

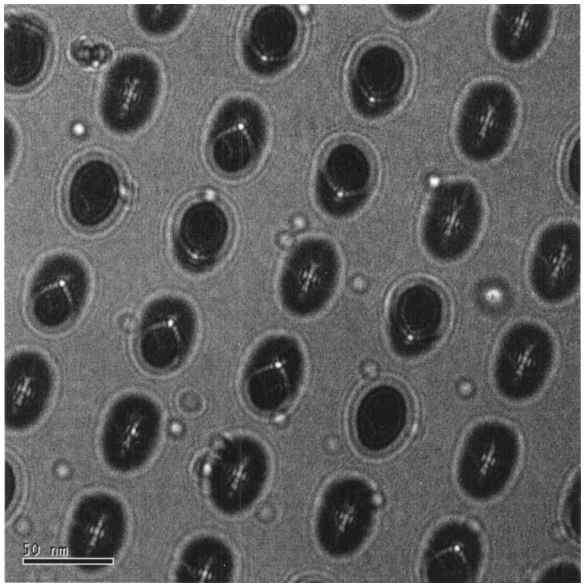

FIG. 9. Wide area Lorentz image showing ellipses in single and double vortex states.

In Fig. 9, we show a wider area LTEM image. In it there are 17 particles in a single vortex state and 10 in the two vortex state. This would appear to contradict the conclusion extracted from the DMOKE data that most ellipses should be in the two vortex state. The two findings can be reconciled by recalling that the ellipses on the silicon nitride window are slightly ($\approx$20%) smaller than those above the Si; smaller particles are expected to favor the one vortex state.[15] There could also be additional complications due to residual fields in the microscope and shape imperfections of the individual particles.

CONCLUSIONS

We have investigated the magnetization reversal in an array of elliptical permalloy elements using the diffracted magneto-optic Kerr effect technique, micromagnetic simulations, and Lorentz electron microscopy. Two different magnetization reversal processes were observed depending on the direction of the applied field: parallel or perpendicular to the long axis of the ellipse. In the first case the analysis of the diffracted loops indicates that the reversal occurs via the nucleation, displacement, and annihilation of two vortices with opposite chirality. In the other case, the reversal was found to occur with the nucleation of a single vortex state.

The nucleation and annihilation fields measured experimentally as a function of the angle between the applied field and the long axis change smoothly with angle with no clear indication of a change from double to single vortex states. Micromagnetic simulations show that, although double and single vortex formation are robust for fields applied along 0° and 90°, at intermediate angles both the nucleation and annihilation processes depend on subtle choices made in the simulation: cell size, field history, and small out of plane fields. It is likely that these effects translate into a distribution of switching mechanisms in the experimental data that mask the transition from single to double vortex formation.

Lorentz electron microscopy images taken at remanence show the existence of both single and double vortex states. Although apparently contradictory, this finding can be reconciled with our MOKE and micromagnetic data by noting that the ellipses on the silicon nitride window are 20% smaller than in the rest of the array. These smaller particles make the single vortex ground state energetically more favorable.[15]

ACKNOWLEDGMENTS

P.V. gratefully acknowledges financial support from MURST-COFIN 2003. Work at ANL was supported by U.S. Department of Energy BES Materials Sciences under Contract No. W-31-109-ENG-38. V.M. was supported by U.S. National Science Foundation, Grant No. NSF ECE-0202780.

[1] See, e.g., *Magnetic Nanostructures*, edited by H. S. Nalwa (American Scientific Publishers, Los Angeles, 2002), and references quoted therein.
[2] N. A. Usov, Ching-Ray Chang, and Zhung-Hang Wei, J. Appl. Phys. **89**, 7591 (2001).
[3] A. Fernandez and C. J. Cerjan, J. Appl. Phys. **87**, 1395 (2000).
[4] P. Vavassori, V. Metlushko, R. M. Osgood, M. Grimsditch, U. Welp, G. Crabtree, W. Fan, S. Brueck, B. Ilic, and P. Hesketh, Phys. Rev. B **59**, 6337 (1999).
[5] M. Grimsditch, I. Guedes, V. Metlushko, P. Vavassori, B. Ilic, P. Neuzil, and R. Kumar, J. Appl. Phys. **89**, 7096 (2001).
[6] I. Guedes, N. Zaluzek, M. Grimsditch, V. Metlushko, P. Vavassori, B. Ilic, P. Neuzil, and R. Kumar, Phys. Rev. B **62**, 11 719 (2000).
[7] I. Guedes, M. Grimsditch, V. Metlushko, P. Vavassori, R. Camley, B. Ilic, P. Neuzil, and R. Kumar, Phys. Rev. B **66**, 014434 (2002).
[8] M. Grimsditch, P. Vavassori, V. Novosad, V. Metlushko, H. Shima, Y. Otani, and K. Fukamichi, Phys. Rev. B **65**, 172419 (2002).
[9] N. J. Zaluzec, J. Microsc. Microanal. **7**, 222 (2001).
[10] H. W. Fuller and M. E. Hale, J. Appl. Phys. **31**, 1699 (1960).
[11] N. J. Zaluzec (unpublished).
[12] OOMMF user's guide (unpublished).
[13] S. C. Whittenburg, in *Magnetic Nanostructures* (Ref. 1), pp. 425–439.
[14] N. A. Usov, Ching-Ray Chang and Zhung-Hang Wei, Phys. Rev. B **66**, 184431 (2002).
[15] K. Yu. Guslienko, V. Novosad, Y. Otani, H. Shima, and K. Fukamichi, Phys. Rev. B **65**, 24414 (2002).